One-Dimensional to Three-Dimensional Ripple-to-Dome Transition for SiGe on Vicinal Si (1 1 10)

B. Sanduijav,[1] D. Scopece,[2] D. Matei,[1] G. Chen,[1,*] F. Schäffler,[1] L. Miglio,[2] and G. Springholz[1,†]

[1]*Institut für Halbleiter- und Festkörperphysik, Johannes Kepler University, A-4040 Linz, Austria*

[2]*L-NESS and Department of Materials Science, Università di Milano-Bicocca, Milano, Italy*

(Received 27 March 2012; published 12 July 2012)

SiGe heteroepitaxy on vicinal Si (1 1 10) is studied as a model system for one-dimensional (1D) to three-dimensional growth mode transitions. By *in situ* scanning tunneling microscopy it is shown that the 1D-3D transition proceeds smoothly from perfectly facetted 1D nanoripples to coarsened superripples, tadpoles, asymmetric domes, and barns without involving coalescence or agglomeration. By extension of the studies to a wide range of SiGe compositions, a 1D-3D growth phase diagram is obtained. Total energy calculations reveal that the observed critical transition volumes are fully consistent with thermodynamic driven strain relaxation.

DOI: 10.1103/PhysRevLett.109.025505 PACS numbers: 81.07.−b, 68.37.Ef, 68.55.A−, 81.15.Hi

SiGe heteroepitaxy on Si surfaces has been intensely studied as a model system for growth instabilities [1–13] and self-organized surface texturing [13–19] on the nanoscale that forms the basis for self-assembled nanostructures. Most of these studies have been devoted to the singular Si (001) surface, on which a spontaneous two-dimensional (2D) to 3D growth mode transition sets in at a certain critical layer thickness [1–12]. On vicinal and high-index surfaces, however, the broken symmetry often leads to the formation of one-dimensional nanostructures, [13–23] by mechanisms such as kinetic step bunching [16,17], step-step interactions [24–26], or spontaneous surface facetation [19,23,27], as has been observed for a wide range of material systems [28–34]. A prominent example is the SiGe/Si (1 1 10) system, where a perfectly facetted 1D ripple structure is formed during the initial stages of growth [20–23]. At higher coverages, however, the growth evolution becomes dictated by the volumetric energy of the system [2–4,9–12]. This induces a strong driving force for coherent 3D island formation and the fundamental question arises how such a 1D-3D growth transition occurs and whether it is at variance to the usual 2D/3D Stranski-Krastanow transition, as has been recently suggested by Persichetti *et al.* [35,36].

To resolve this issue, we present an extensive study of the 1D-3D transition of SiGe on Si (1 1 10) over a wide range of compositions and coherent growth conditions. By scanning tunneling microscopy (STM), we show that the transformation proceeds smoothly via geometrically distinct phases, starting from coarsened ripples over frustrated tadpole islands to multifacetted domes and barns, whose structure is revealed in all details by STM. The onset of the 1D-3D transition is characterized by a shrinking of the ripple length and simultaneous vertical and lateral expansion. Subsequent transformation into domes and barns is dictated by volumetric strain relaxation as shown by total energy calculations, but no evidence for clustering or agglomeration is found. We provide a 1D-3D growth phase diagram as a function of SiGe composition, and overall excellent agreement between experiments and theory is found.

The investigations were performed in a multichamber molecular beam (MBE) and STM system, enabling surface imaging and growth without breaking ultrahigh vacuum conditions [20,23]. Complementing experiments in a Riber SIVA-45 MBE system [12–22] produced the same results in all cases. Vicinal Si (1 1 10) substrates miscut by 8° with respect to (001) were prepared by device-grade chemical cleaning [16] and a 40 nm thick Si buffer was grown after oxide desorption. As proven by STM, this produces very clean and smooth starting surfaces, consisting of a highly regular double monolayer (ML) step structure perpendicular to the miscut direction [23]. Ge or $Si_{1-x}Ge_x$ layers were deposited at 1–2 Å/min and a substrate temperature of 600 °C which is somewhat higher than the 550 °C used in our previous experiments [23] in order to promote the 1D-3D transition. The layer thicknesses and compositions were varied over a wide range from $x_{Ge} = 0.2$ to 1. After growth, the samples were rapidly quenched to room temperature and transferred for STM investigations. Equilibrium surface morphologies were derived from *in situ* annealing experiments.

Ge growth on Si (1 1 10) results in perfect 1D faceting of the surface at a critical coverage of 4.2 ML [23]. As a result, the surface is completely covered by ~20 nm wide and ~200 nm long nanoripples running along the $[55\bar{1}]$ miscut direction as demonstrated by Fig. 1(a). The ripples show a high degree of uniformity and their prismatic shape is defined by perfect {105} side facets. This is revealed by the high-resolution STM image of Fig. 1(c) and leads to a significant lowering of the surface energy [23,27]. Perfect faceting is also proven by the surface orientation map (SOM) [15] depicted as an inset, where only two well-defined {105} facet spots appear.

As shown by Fig. 1(b), when the Ge coverage increases above 5 ML, a 1D-3D growth mode transition sets in and isolated superripples and 3D islands appear on the surface. The superripples, labeled "1" and "2" in Fig. 1(b), exhibit

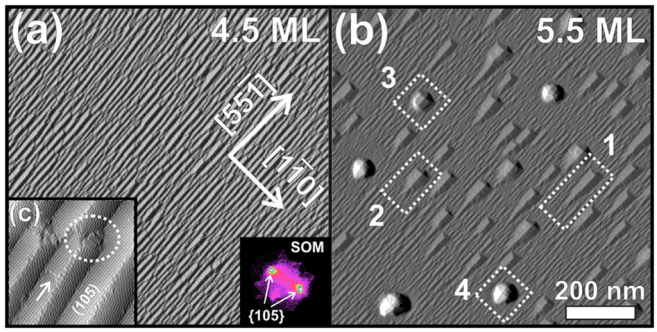

FIG. 1 (color online). STM images of Ge deposited on Si (1 1 10) before (a) and after (b) the 1D-3D ripple-to-dome transition at 4.5 and 5.5 ML coverage, respectively. The surface orientation map (SOM) inset and the high-resolution STM image in (c) reveals complete {105} facetation. The successive stages of the ripple-to-dome transition are indicated by the labels from "1" to "4" and corresponding high-resolution STM images are shown in Fig. 2.

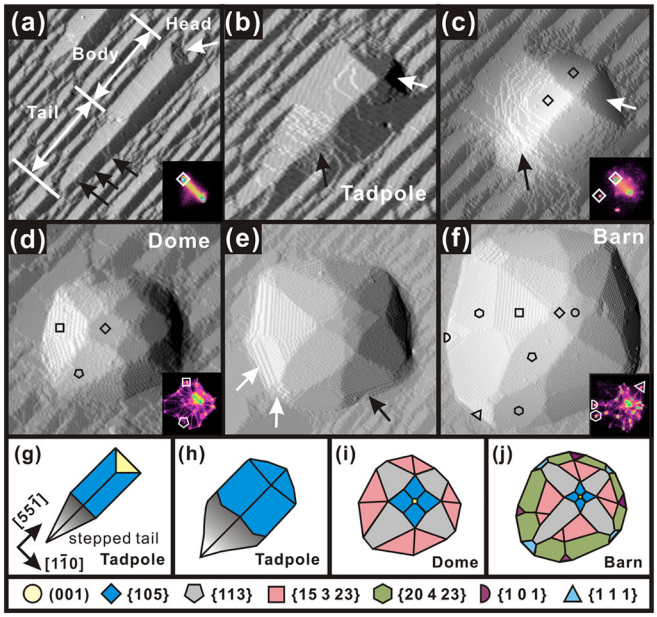

FIG. 2 (color online). High-resolution STM images showing the evolution of from ripples, to tadpoles, domes, and barns with increasing island volume: (a) Coarsened superripple with (001) facet termination, (b) tadpole with V-shaped tail and {105} faceted head, (c) transitional island between tadpoles and domes, (d) fully developed dome with {113} and {15 3 23} facts, (e) transitional barn with densely stepped edges, and (f) fully developed barn with steep {101}, {20 4 23}, and {111} facets. Image size: 100×100 nm^2. Different facets are indicated by the symbols and colors in the models shown in (g) to (j). The insets show the surface orientation maps of the STM images.

a highly asymmetric tadpolelike shape with thickened head and tapered tail. Their height and width is increased by a factor of 3 to $h \sim 3.5$ nm and $b \sim 50$ nm but their aspect ratio $A = h/b = 0.07$ remains unchanged due to the persisting {105} sidewall facetation. The larger islands labeled "3" and "4" are more rounded and significantly enlarged in height to $h \sim 6.5$ nm, resulting in a concomitant threefold increase in aspect ratio. Their shapes resemble those of domes [3,4] and barns [10,11] seen on Si (001), but display a significant asymmetry due to the 8° miscut of the underlying (1 1 10) surface. From Fig. 1(b) it is clear that the ripple-to-dome transformation proceeds via coherent coarsening of single ripples and islands and not by clustering and agglomeration as proposed by Persichetti *et al.* [35,36].

The individual stages of the successive ripple-to-dome transition are presented in Fig. 2 in high resolution. Already before the onset of island nucleation, ripple bifurcation occurs, as indicated by the circle in Fig. 1(c). Since 1D ripples with uniform cross section can only elastically relax strain perpendicular to the ripple axis, the longitudinal strain component is completely preserved [22,27]. Hence, ripple disruption by bifurcation and formation of local (001) facets becomes favorable with increasing Ge deposition. On the {105} ripple facets, atomic steps [arrows in Fig. 1(c)] provide a mechanism for lateral ripple expansion via step flow growth. Figure 2(a) shows the zoomed-in STM image of the first superripple that represents the precursor state for island nucleation. It is shortened and 3 times widened compared to the initial ripples. Its tadpole shape is composed of three parts [see Figs. 2(a) and 2(g)], namely, a {105} bound prism body, an abrupt (001) terminated head, and a long "V"-shaped tail that narrows along the $[\bar{5}\,\bar{5}\,1]$ direction through dense step bunching along the ripple facets.

Further coarsening leads to an enhanced tadpole growth in the transversal and vertical direction accompanied by a successive shrinking of the tail in the longitudinal direction. This is demonstrated by Figs. 2(a) and 2(b), representing two subsequent coarsening stages of the tadpole islands. In this process, Ge is sucked from the tail into the body for more efficient strain relief. At a certain critical body width of 40 nm, two additional {105} facets appear at the tadpole head [cf. Figs. 2(b) and 2(h)], replacing the initial (001) facet. Thus, an asymmetric tilted pyramid is formed. The stark asymmetry between the upper and lower tadpole termination arises from the geometrical frustration due to the 8° substrate miscut, for which reason no low-energy shallow facet is available for tail termination. Thus, material transfer from the tail to the body can be accommodated only by step bunching in the tail region, as indicated by the black arrow in Fig. 2(b).

In the next evolution step, the tadpole tail is completely absorbed into the body. This is shown by Fig. 2(c) [island "3" in Fig. 1(b)], where the tadpole body is now nearly fully terminated by four adjacent {105} facets. At this point, a substantial vertical growth sets in without much lateral expansion. As revealed by STM, this proceeds via ML nucleation at the tadpole top and downward step flow growth, resulting in pronounced step bunching also at the lateral tadpole edges. At a certain critical tadpole size, these step bunches transform abruptly into steeper facets

and thus, a fully facetted dome is formed. This is demonstrated in Fig. 2(d) by the STM image of the dome island "4", which is composed of four {113} and eight {15 3 23} side facets in addition to {105}, as confirmed by the corresponding SOM inset. The aspect ratio of the dome islands is increased to $A = 0.21$. Thus, volumetric strain relaxation becomes the dominating factor at this growth stage. Because of the vicinal substrate orientation, the domes are asymmetric, featuring significantly reduced {113} and {15 3 23} facets in the miscut direction, as illustrated by the geometrical model displayed in Fig. 2(i).

Further coarsening leads to a third transition from domes to barns with even steeper side facets. Figure 2(e) represents a transitional island with intermediate shape, evidencing that again steeper side facet nucleation proceeds via step bunching at the perimeter of the domes. The final, fully developed barn displayed in Fig. 2(f) features additional {20 4 23}, {101}, and {111} side facets (see SOM inset) with inclinations up to 60°. Evidently, the transformation into barns is driven by the higher degree of strain relief provided by the increased $A \sim 0.25$ aspect ratio. As indicated by Fig. 2(j), the barns also exhibit four {101} corner facets not seen for barns on Si (001) [10,11,37].

Based on the results of Figs. 1 and 2, the evolution from ripples to tadpoles, domes, and barns neither involves aggregation, clustering or bunching of islands, contrary to what has been reported by Persichetti *et al.* [35,36]. Moreover, while the smooth tadpole formation from 1D ripples completely differs from the nucleation of isolated Ge pyramids on planar Si (001) substrates [5–8], the obvious analogy of the later dome to barn transition [10,11] is clear evidence that volumetric strain relaxation rather than anisotropic island-island interactions [35,36] governs the coarsening at this growth stage. This is quite expected because the up to 60° side wall inclinations of the domes and barns much exceed the 8° miscut of (1 1 10) with respect to (001). Although the different results of Persichetti *et al.* [35,36] could have been caused by their 1 order of magnitude lower Ge growth rate, our finding that island agglomeration does not occur even upon postgrowth annealing suggests that this is rather due to the different substrate preparation, where in our case all extrinsic island nucleation sources were effectively eliminated by Si buffer deposition, as was checked by STM control experiments.

To systematically map out the strain dependence of the ripple-to-dome transition, a complete series of SiGe samples with varying x_{Ge} from 0.2 to 1 was grown. To push the morphologies close to thermal equilibrium, the samples were *in situ* annealed at 600 °C for 15 min after growth. As a general trend, at lower x_{Ge} the ripple-to-dome transition is shifted to higher coverages. Therefore, SiGe layers of up to 100 ML are required to induce the 1D-3D growth transition. Figures 3(a) and 3(b) present the results for $x_{Ge} = 0.25$ at 20 and 60 ML, respectively. At 20 ML, even after annealing, the surface exclusively contains stable (001)-headed tadpoles with ~600 nm length and ~50 nm width, whereas at 60 ML solely dome islands appear. Both exhibit the same overall shapes as reported in Fig. 2, except for the nearly tenfold increase in size. Moreover, at intermediate coverages (not shown), a similar coexistence of tadpoles and domes is found.

For the pure Ge case, STM images at 5 and 6.7 ML are depicted in Figs. 3(c) and 3(d), showing that even after annealing, at 5 ML the surface exclusively contains ripples and (001) headed tadpole islands, whereas at higher coverage only dome islands remain with no indication of clustering or agglomeration. Even up to coverages of 7.5 ML, the surface still contains merely dome and barn islands; i.e., only a negligible number of them (less than 3%) have evolved into superdomes due to dislocation formation. On the contrary, Persichetti *et al.* [35,36] have found dislocated islands already at the early stages of growth, which is an indication that heterogeneous island nucleation occurred in their experiments.

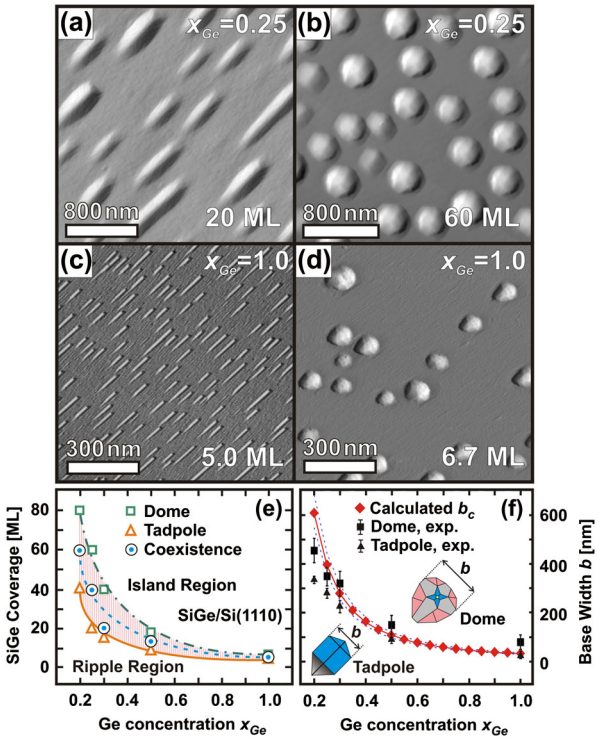

FIG. 3 (color online). SiGe layers on Si (1 1 10) after postgrowth annealing for $x_{Ge} = 0.25$ (a),(b) and $x_{Ge} = 1$ (c),(d) at coverages below and above the ripple-to-dome transition. Note the different scale of the images. (e) Equilibrium phase diagram for the 1D-3D transition derived from the annealing experiments, representing the stability regions for the different phases. (f) Comparison of the experimental average base width of tadpoles (triangles) and domes (black) with the critical base widths b_c (diamonds) derived from total energy calculations. The dotted lines indicate the theoretical variation of b_c obtained when the less known facet, edge, and step energies are varied.

The thermodynamic growth phase diagram compiled from the annealing experiments is presented in Fig. 3(e). It shows the stability regions for ripples, tadpoles, and domes as a function of SiGe coverage and Ge concentration. Below the solid line, solely ripples or tadpoles are observed, at intermediate coverages (shaded region) there is a small coexistence region for tadpoles and domes, and at higher coverages (dash-dotted line) only dome islands remain. This sequence is identical for all Ge concentrations, but the required critical coverage for the 1D-3D transitions strongly rises with decreasing Ge content x_{Ge}, similar to usual SK systems [13,38]. As shown in Fig. 3(f), also the island sizes for the tadpole-to-dome transition strongly increases with decreasing x_{Ge}, scaling in a similar way as the critical coverage.

To theoretically predict the critical size for the tadpole-to-dome transition, we have devised a total energy model [9,12] that allows the comparison of the energy of the tadpoles (T) to that of domes (D) equal in volume. Since in the experiments it was found that at the 1D-3D transition the tadpole width is equal to the width of the domes, a one-to-one correspondence in volume is obtained by adjusting the tadpole length. The total energy of the tadpoles E_T and domes E_D with respect to that of a generic wetting layer (WL) E_{WL} was computed for the island geometries derived by STM using

$$E_T - E_{\mathrm{WL}} = V(\rho_T - \rho_{\mathrm{WL}}) + (S_{TT}\gamma_{TT} + S_{TB}\gamma_{TB} + S_{TH}\gamma_{TH}) - B_T\gamma_{\mathrm{WL}} + L_T\Gamma, \quad (1)$$

$$E_D - E_{\mathrm{WL}} = V(\rho_D - \rho_{\mathrm{WL}}) + S_D\gamma_D - B_D\gamma_{\mathrm{WL}} + L_D\Gamma. \quad (2)$$

In both equations, the first term accounts for the volumetric elastic energy relaxation within the tadpoles or domes that is proportional to the volume V times the average elastic energy density ρ, computed by finite element calculations using *ab initio*-derived elastic constants [39,40]. The second term describes the increase in surface energy due to the exposed surfaces of the tadpole tail (TT), body (TB), and head (TH) or domes (D), where γ_i and S_i represent the corresponding surface energy densities and surface areas. The energy of {105} facets was obtained from *ab initio* data [27], giving ≈ 57 meV/Å^2, which is kept constant for any alloying because Ge surface segregation is expected in all cases. For the surface energy of the domes, we use an average value of 65 meV/Å^2, as derived by our previous works [12]. For the tadpoles, a γ value between 60–63 meV/Å^2 is estimated [41] for the (001) tadpole head, giving, however, no significant variation of the final results. Negligible changes were similarly produced when accounting for the cumulative effect of steps on the tadpole tails through an extra surface energy term up to 5 meV/Å^2. The third term represents the energy of the WL that is reduced when an area B is covered by the base of the islands, where we take the faceting condition [27] as the reference for γ_{WL}. The last term, finally, accounts for the edge energy costs Γ at the facet borders, which is varied between 100–370 meV/Å, according to our experimentally confirmed estimations [23].

The evolution of the total energy of the tadpoles and domes as a function of base width is presented in Fig. 4 for three different Ge concentrations $x_{\mathrm{Ge}} = 0.25$, 0.5, and 1.0 as indicated. For all cases, a crossover between tadpole and dome energy occurs at a certain critical size b_c as indicated by the arrows. Beyond this size the domes are energetically favored. Comparing the curves for different x_{Ge}, evidently, the critical size strongly increases with decreasing Ge content from $b_c = 30$ nm for $x_{\mathrm{Ge}} = 1$ to 400 nm for $x_{\mathrm{Ge}} = 0.25$, scaling roughly as $b_c \sim \varepsilon^{-2}$. The complete dependence of the critical tadpole size is presented in Fig. 2(f), demonstrating that the theoretical (diamonds) and experimental values (squares and triangles) are in nice agreement with each other. Thus, volumetric elastic relaxation is the key driving force for dome formation. A variation of parameters such as facet and edge energies as well as extra energy costs for steps on the tadpole tails does not influence significantly the theoretical results, as indicated by the dotted lines. Only for low Ge content $x_{\mathrm{Ge}} \leq 0.25$ a modest theoretical overestimation of b_c is found, which is attributed to the assumption that the surface energy is fully determined by Ge segregation even at low x_{Ge}, where also kinetic limitations will delay the transition process. Kinetics may also account for the finite tadpole-dome coexistence region in the phase diagram.

In conclusion, a novel 1D-3D growth transition of SiGe on vicinal Si (1 1 10) was unraveled by high-resolution scanning tunneling microscopy. The initial 1D ripple transformation proceeds smoothly by transversal expansion and longitudinal shrinking, which completely differs from the abrupt island nucleation process on planar 2D surfaces. Further coarsening occurs via several geometrically distinct phases, from superripples, to tadpole islands, to finally

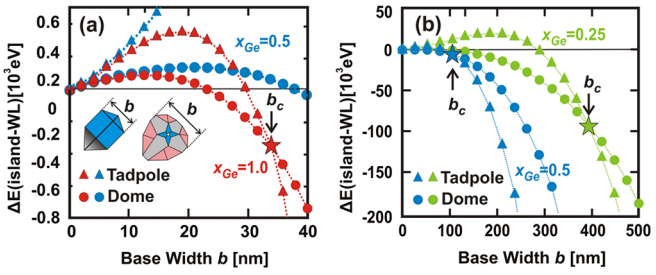

FIG. 4 (color online). Calculated relative total energies $\Delta E = E_{\mathrm{isl}} - E_{\mathrm{WL}}$ of the tadpoles and domes as a function of base width b for $x_{\mathrm{Ge}} = 0.25$, 0.5, and 1.0 as indicated. The corresponding geometries were constructed based on the STM images of Fig. 2 and a perfectly {105} facetted wetting layer was assumed. The arrows indicate the critical base widths b_c where the dome energy becomes lower than that of the tadpoles.

multifacetted asymmetric domes and barns as the aspect ratio increases. This is governed by elastic strain relaxation, in perfect agreement with total energy calculations. Extending our studies to a wide range of SiGe compositions and postgrowth annealing experiments, a complete thermodynamic growth phase diagram for the ripple-to-dome transition was derived. Our results not only provide a key reference for further investigations, but also apply for a wide range of material systems and vicinal surfaces, where the formation of 1D nanostructures often occurs.

We gratefully acknowledge discussions with Francesco Montalenti and support by the Austrian Science Funds (P14684, SFB025), Austrian NanoInitiative, and Cariplo Foundations.

*gang.chen@jku.at
†gunther.springholz@jku.at

[1] Y. W. Mo, D. E. Savage, B. S. Swartzentruber, and M. G. Lagally, Phys. Rev. Lett. **65**, 1020 (1990).
[2] J. Tersoff and F. K. LeGoues, Phys. Rev. Lett. **72**, 3570 (1994).
[3] F. Ross, R. M. Tromp, and M. C. Reuter, Science **286**, 1931 (1999); F. M. Ross, J. Tersoff, and R. M. Tromp, Phys. Rev. Lett. **80**, 984 (1998).
[4] G. Medeiros-Ribeiro, A. M. Bratkovski, T. I. Kamins, D. A. A. Ohlberg, and R. S. Williams, Science **279**, 353 (1998).
[5] A. Vailionis, B. Cho, G. Glass, P. Desjardins, D. G. Cahill, and J. E. Greene, Phys. Rev. Lett. **85**, 3672 (2000).
[6] P. Sutter, E. Sutter, and L. Vescan, Appl. Phys. Lett. **87**, 161916 (2005).
[7] A. Rastelli, H. Von Känel, B. J. Spencer, and J. Tersoff, Phys. Rev. B **68**, 115301 (2003); J. Tersoff, B. J. Spencer, A. Rastelli, and H. von Känel, Phys. Rev. Lett. **89**, 196104 (2002).
[8] B. Voigtländer, Surf. Sci. Rep. **43**, 127 (2001).
[9] F. Montalenti *et al.*, Phys. Rev. Lett. **93**, 216102 (2004).
[10] E. Sutter, P. Sutter, and J. E. Bernard, Appl. Phys. Lett. **84**, 2262 (2004).
[11] M. Stoffel, A. Rastelli, J. Tersoff, T. Merdzhanova, and O. G. Schmidt, Phys. Rev. B **74**, 155326 (2006).
[12] M. Brehm *et al.*, Phys. Rev. B **80**, 205321 (2009).
[13] I. Berbezier and A. Ronda, Phys. Rev. B **75**, 195407 (2007); Surf. Sci. Rep. **64**, 47 (2009).
[14] Y. H. Phang, C. Teichert, M. G. Lagally, L. J. Peticolos, J. C. Bean, and E. Kasper, Phys. Rev. B **50**, 14 435 (1994).
[15] C. Teichert, Phys. Rep. **365**, 335 (2002).
[16] C. Schelling, G. Springholz, and F. Schäffler, Phys. Rev. Lett. **83**, 995 (1999); C. Schelling, M. Mühlberger, G. Springholz, and F. Schäffler, Phys. Rev. B **64**, 041301(R) (2001).
[17] J. Mysliveček, C. Schelling, F. Schäffler, G. Springholz, P. Šmilauer, J. Krug, and B. Voigtländer, Surf. Sci. **520**, 193 (2002).
[18] Jian-hong Zhu, K. Brunner, and G. Abstreiter, Appl. Phys. Lett. **73**, 2438 (1998); A. A. Darhuber, J. Zhu, V. Holý, J. Stangl, P. Mikulík, K. Brunner, G. Abstreiter, and G. Bauer, Appl. Phys. Lett. **73**, 1535 (1998).
[19] Y. Kim, M. H. Jo, T. C. Kim, C. W. Yang, J. W. Kim, J. S. Hwang, D. Y. Noh, N. D. Kim, and J. W. Chung, Phys. Rev. Lett. **102**, 156103 (2009).
[20] B. Sanduijav, D. Matei, G. Chen, and G. Springholz, Phys. Rev. B **80**, 125329 (2009).
[21] L. Persichetti, A. Sgarlata, M. Fanfoni, and A. Balzarotti, Phys. Rev. Lett. **104**, 036104 (2010).
[22] G. Chen, E. Wintersberger, G. Vastola, H. Groiss, J. Stangl, W. Jantsch, and F. Schäffler, Appl. Phys. Lett. **96**, 103107 (2010); G. Chen, G. Vastola, J. J. Zhang, B. Sanduijav, G. Springholz, W. Jantsch, and F. Schäffler, Appl. Phys. Lett. **98**, 023104 (2011).
[23] G. Chen, B. Sanduijav, D. Matei, G. Springholz, D. Scopece, M. J. Beck, F. Montalenti, and L. Miglio, Phys. Rev. Lett. **108**, 055503 (2012).
[24] J. Tersoff, Y. H. Phang, Zhenyu Zhang, and M. G. Lagally, Phys. Rev. Lett. **75**, 2730 (1995); Feng Liu, J. Tersoff, and M. G. Lagally, Phys. Rev. Lett. **80**, 1268 (1998).
[25] Mina Yoon, H. N. Lee, W. Hong, H. M. Christen, Z. Zhang, and Z. Suo, Phys. Rev. Lett. **99**, 055503 (2007).
[26] Y.-M. Yu, A. Voigt, X. Guo, and Y. Liu, Appl. Phys. Lett. **99**, 263106 (2011).
[27] D. Scopece, F. Montalenti, and M. J. Beck, Phys. Rev. B **85**, 085312 (2012).
[28] S. H. Lee and G. B. Stringfellow, Appl. Phys. Lett. **73**, 1703 (1998).
[29] W. Ma, R. Nötzel, A. Trampert, M. Ramsteiner, H. Zhu, H.-P. Schönherr, and K. H. Ploog, Appl. Phys. Lett. **78**, 1297 (2001).
[30] T. Nitta, Y. Ohno, S. Shimomura, and S. Hiyamizu, J. Vac. Sci. Technol. B **19**, 1824 (2001).
[31] M. Hanke, Zh. M. Wang, Yu. I. Mazur, J. H. Lee, G. J. Salamo, and M. Schmidbauer, Appl. Phys. Lett. **92**, 033111 (2008); V. Yadzanpanah, Z. M. Wang, J. H. Lee, and G. J. Salamo, New J. Phys. **8**, 233 (2006).
[32] A. L.-S. Chua, E. Pelucchi, A. Rudra, B. Dwir, E. Kapon, A. Zangwill, and D. D. Vvedensky, Appl. Phys. Lett. **92**, 013117 (2008).
[33] Masahiro Fujii, Satoru Tanaka, Phys. Rev. Lett. **99**, 016102 (2007).
[34] F. Sánchez, G. Herranz, J. Fontcuberta, M. V. García-Cuenca, C. Ferrater, and M. Varela, Phys. Rev. B **73**, 073401 (2006).
[35] L. Persichetti, A. Sgarlata, M. Fanfoni, and A. Balzarotti, Phys. Rev. B **82**, 121309 (2010).
[36] L. Persichetti, A. Sgarlata, M. Fanfoni, and A. Balzarotti, Phys. Rev. Lett. **106**, 055503 (2011).
[37] M. Brehm, H. Lichtenberger, T. Fromherz, and G. Springholz, Nanoscale Res. Lett. **6**, 70 (2011) [http://www.nanoscalereslett.com/content/6/1/70].
[38] D. V. Yurasov and Yu. N. Drozdov, Semiconductors **42**, 563 (2008).
[39] The elastic energy density of a planar WL is around 1.6 meV/Å3.
[40] J. J. Zhang *et al.*, Phys. Rev. Lett. **105**, 166102 (2010).
[41] G. Lu, M. Cuma, and F. Liu, Phys. Rev. B **72**, 125415 (2005).